American Mineralogist, Volume 79, pages 862–877, 1994

Composition and temperature dependence of Fe-Mg ordering in cummingtonite-grunerite as determined by X-ray diffraction

MARC HIRSCHMANN,* BERNARD W. EVANS, HEXIONG YANG
Department of Geological Sciences AJ-20, University of Washington, Seattle, Washington 98195, U.S.A.

ABSTRACT

The crystal structures of 24 heat-treated and six unheated natural ferromagnesian clinoamphiboles have been refined from single-crystal X-ray intensity data. Relative to Mg, Fe^{2+} is strongly concentrated in the M4 site and weakly depleted in the M2 site in all crystals examined, but the degree of fractionation is less pronounced in the samples equilibrated at high temperature. Fe shows a weak preference for M3 relative to M1 in heat-treated cummingtonite-grunerite, but no significant preference is observed in unheated crystals. Site preferences expressed in terms of an ideal ordering energy, $-RT \ln K_{ij}$, show no temperature dependence over the range of temperatures of heat treatment, 600–750 °C. The ideal ordering energy between M1 and M4, $-RT \ln K_{14}$, equal to 18.2 ± 0.3 (1σ) kJ, is independent of composition except for very magnesian compositions, for which the degree of ordering decreases. The ideal ordering energy between the M1 and M2 sites, $-RT \ln K_{12}$, decreases from −2 kJ at pure $Fe_7Si_8O_{22}(OH)_2$ to −6 kJ at pure $Mg_7Si_8O_{22}(OH)_2$. With the assumption that Ca is restricted to the M4 site and that Mn is strongly ordered into the M4 site, M123 vs. M4 site preferences determined by Mössbauer spectroscopy are consistent with our X-ray diffraction results. The projection of Mössbauer results to the Fe-Mg join is more critically dependent than X-ray refinements on the assignment of Ca and Mn onto the appropriate sites. Our projection of the Mössbauer data of natural cummingtonite and grunerite collected by Hafner and Ghose (1971) indicates stronger ordering between M4 and M123 than previously interpreted.

At room temperature, heat-treated cummingtonite with Fe/(Fe + Mg) as great as 0.38 has $P2_1/m$ symmetry. Average bond lengths for the M1, M2, and M3 octahedra correlate well with mean ionic radius, and, for equivalent site occupancies, the mean bond length of the M3 octahedron is approximately 0.05 Å smaller than those of the M1 and M2 octahedra. When corrected for impurities, variations in cell volume with Fe/(Fe + Mg) are linear, giving extrapolated molar volumes of 26.33 ± 0.01 (1σ) J/bar for magnesiocummingtonite and 27.84 ± 0.01 J/bar for grunerite. The cell volume of ferromagnesian clinoamphibole is indistinguishable from that of orthoamphibole of the same composition, indicating that cummingtonite molar volumes may also be appropriate for end-member anthophyllite and ferroanthophyllite. The derived molar volume of anthophyllite is 1% smaller than that given by the data bases of Berman (1988) and Holland and Powell (1990). There are no detectable variations in cell volume of cummingtonite attributable to changes in ordering state.

INTRODUCTION

Because of their common occurrence and compositional complexity, amphiboles are potentially among the most powerful petrogenetic indicators. Given appropriate understanding of their chemical content, amphiboles may be applied as thermobarometers, fluid fugacity monitors, and, through documentation of intracrystalline site occupancies, indicators of cooling rates. Unfortunately, compositional and structural complexities have hindered the development of quantitative descriptions of the energetics of amphibole solutions. One of the constraints required for rigorous thermodynamic and kinetic models of amphibole behavior is a detailed description of intracrystalline ordering as a function of temperature, pressure, and amphibole composition. In this study, we use single-crystal X-ray diffraction to determine site occupancies as a function of composition and temperature for natural clinoamphiboles close to the magnesiocummingtonite-grunerite binary, $(Mg,Fe)_7Si_8O_{22}(OH)_2$. These determinations provide much of the information necessary to model the mixing properties of ferromagnesian clinoamphibole. Site-occupancy determinations along this

* Present address: Division of Geological and Planetary Sciences 170-25, California Institute of Technology, Pasadena, California 91125, U.S.A.

0003–004X/94/0910–0862$02.00

TABLE 1. Sample localities, heat treatments, and references

Specimen no.	Rock type	Fe/(Fe + Mg) (%)	No. of crystals heat-treated at T (°C)* 600	700	750	Location	References
KL14A	cum-tr-ol rock	11	45a			Feather River, California	1, U. Wash. collection
W82-009	metas. cum rock	22	57d	30a		Watkins Fjord, Greenland	2, U. Wash. collection
USNM 118125	metas. cum rock	35–38	11a	1c	8a**	Baltimore Co., Maryland	3, 4, 5, 6
DH7-482	iron formation	38–39		21a		Bloom Lake, Quebec	5, 7, 8, 9, 11, 12, 13, 14
DH10-95	iron formation	46		6b		Bloom Lake, Quebec	8, 9, 11, 12
DH7-484	iron formation	49	14a,14g	4a,4b		Bloom Lake, Quebec	8, 9
DH10-85	iron formation	55		17c		Bloom Lake, Quebec	8, 9
10-K	iron formation	59		18a		Labrador City, Labrador	9, 10, 11
AMNH 27022	iron formation	58–60		3b		Montenevoso, Alto Adige, Italy	
Lab 510	iron formation	61		2b		Wind River Mts., Wyoming	15, U. Wash. collection
7B	iron formation	66		19a		Bloom Lake, Quebec	8, 9, 11, 12
AMNH 24159	iron formation	66–70	12a	5b,5c	9a**	Mikonui R., Westland, N.Z.	3, 4, 16
CL-1	iron formation	74		16a		Bloom Lake, Quebec	8, 9
1-K	iron formation	89	15b	22f		Labrador City, Labrador	3, 4, 9, 10, 11, 17

Note: USNM = United States National Museum, Washington, DC. AMNH = American Museum of Natural History, New York. References: (1) Stop 14, Field Guide: Paleozoic-Mesozoic Rocks of the Northern Sierra Nevada, GSA Cordilleran Section, 1977; (2) Watkins Fjord, Kangerdlugssuaq, E. Greenland (S. Hoffman collection); (3) Burns and Strens (1966); (4) Bancroft et al. (1967); (5) Ghose and Weidner (1972); (6) Walter and Salisbury (1989); (7) Ghose (1961); (8) Mueller (1960); (9) Hafner and Ghose (1971); (10) Klein (1964); (11) Klein and Waldbaum (1967); (12) Viswanathan and Ghose (1965); (13) Fischer (1966); (14) Mitchell et al. (1971); (15) Barrus (1970); (16) Mason (1953); (17) Finger (1969).

* Heated crystals are identified in Tables 2–7 and in the text by these numbers, which were assigned during heat treating and crystal selection. Unheated crystals are identified by their specimen numbers.

** Crystals lost during polishing. Averaged microprobe analyses of 1c and 11a were used for the 8a constrained refinement and 5b, 5c, and 12a were used for the 9a constrained refinement.

compositionally simple join can also provide a foundation for understanding ordering and thermodynamic mixing properties of more complex amphiboles, such as anthophyllite, gedrite, and actinolite.

Single-crystal X-ray structure refinements of natural members of the cummingtonite series (Ghose, 1961; Fischer, 1966; Finger, 1969; Ghose and Ganguly, 1982) have shown that Fe^{2+} strongly prefers the M4 site, Mg prefers M2, and the M1 and M3 sites have similar site occupancies. Mössbauer spectra taken at 298 and 77 K do not separately resolve M1, M2, and M3, but they confirm the strong preference of Fe^{2+} for M4 (Bancroft et al., 1967; Hafner and Ghose, 1971; Buckley and Wilkins, 1971; Barabanov and Tomilov, 1973); they have also shown that ordering between M4 and M123 (M123 = combined M1, M2, and M3) is temperature dependent (Ghose and Weidner, 1972). The combination of Mössbauer and infrared absorption spectroscopy also shows that Fe^{2+} favors M13 over M2 (Bancroft et al., 1967; Buckley and Wilkins, 1971; Ying et al., 1989).

In the present work, we confirm the relative site preferences determined previously and document quantitatively the variations in M-site occupancies of cummingtonite as a function of composition and temperature. Measured site occupancies indicate that a three-site model (M13, M2, M4) is required to describe the configurational entropy of cummingtonite accurately. Because of the uneven number of different M sites in the formula unit (two M1, two M2, one M3, two M4), the configurational entropy of cummingtonite is an asymmetric function of composition and cannot be described effectively by a purely macroscopic model of solution energetics. In a forthcoming contribution, the site occupancies reported here will be used to guide the formulation of a microscopic model for the entropy of mixing of ferromagnesian amphibole and, combined with constraints from heterogeneous phase equilibria, will be employed to calibrate simple amphibole mixing properties.

Two commonly applied techniques for determining site occupancies in minerals are single-crystal X-ray diffraction and Mössbauer spectroscopy. Both techniques have advantages and disadvantages, and both have been applied toward understanding ordering in amphiboles. Direct comparison of the two techniques applied to orthopyroxene raises the possibility that there may be systematic differences between site occupancies determined by Mössbauer spectroscopy and those determined by X-ray diffraction (Domeneghetti and Steffen, 1992; Skogby et al., 1992). Such systematic differences may be compounded in amphiboles, where additional uncertainties arise from the role of minor substituents such as Ca, Mn, Al, and Fe^{3+}. The present work provides an opportunity to investigate possible systematic differences between these two techniques for site-occupancy determinations in amphiboles. With this in mind, Dyar and Grant (personal communication) have acquired Mössbauer spectra from many of the samples examined in this study.

EXPERIMENTAL PROCEDURES

Specimen preparation

Samples selected for this investigation (Table 1) include several used in previous Mössbauer (Hafner and Ghose, 1971; Ghose and Weidner, 1972) and other investigations of the monoclinic ferromagnesian amphiboles. The cummingtonite and grunerite samples are all from banded iron formations, and the magnesiocummingtonite samples are from ultramafic rocks (Table 1). These amphiboles tend to be close to binary in composition; significant impurities are MnO, CaO, and in a few

TABLE 2. Microprobe analyses and cation proportions

Wt%	DH7-482	DH7-484	27022	Lab 510	24159	1-K	45a	57d	11a	14a	14g	12a	15b
SiO_2	54.57	53.72	52.51	51.59	50.85	48.94	59.18	57.98	55.40	53.31	53.82	50.82	49.53
TiO_2	0.00	0.00	0.00	0.02	0.01	0.01	0.02	0.01	0.01	0.01	0.01	0.01	0.01
Al_2O_3	0.25	0.13	0.18	1.00	0.40	0.15	0.15	0.69	0.26	0.14	0.15	0.28	0.15
FeO*	21.53	26.88	31.43	33.09	34.78	44.86	7.05	13.11	21.03	26.24	26.81	35.90	44.35
MgO	18.91	16.02	12.62	11.74	9.97	3.16	30.66	25.33	19.62	15.69	15.94	8.91	3.20
MnO	1.58	1.63	0.74	0.99	1.03	0.62	0.22	0.39	0.54	1.60	1.58	0.96	0.60
CaO	0.81	0.41	0.23	0.11	0.33	0.33	0.62	0.73	0.70	0.55	0.46	0.26	0.36
Na_2O	0.02	0.02	0.07	0.06	0.04	0.04	0.07	0.10	0.01	0.01	0.01	0.01	0.06
K_2O	0.02	0.01	0.00	0.02	0.05	0.01	0.01	0.00	0.01	0.01	0.01	0.01	0.01
H_2O†		1.77	1.90	1.65	1.81	1.65			2.03	1.77	1.77	1.81	1.65
F‡			0.12										
Cl	0.00	0.00	0.00	0.00	0.00	0.14	0.01	0.00	0.00	0.03	0.05	0.00	0.14
Less O = F,Cl	0.00	0.00	0.05	0.00	0.00	0.03	0.00	0.00	0.00	0.01	0.01	0.00	0.03
Total	97.69	100.59	99.75	100.27	99.27	99.88	97.99	98.34	99.61	99.35	100.60	98.97	100.03
Tetrahedral cations (normalized to sum of 8)													
Si	7.971	7.985	7.979	7.880	7.951	7.981	7.984	7.926	7.971	7.984	7.983	7.966	7.981
$^{[4]}Al$	0.029	0.015	0.021	0.120	0.049	0.019	0.016	0.074	0.029	0.016	0.017	0.034	0.019
M-site cations (normalized to sum of 7)													
$^{[6]}Al$	0.014	0.007	0.011	0.059	0.024	0.010	0.008	0.038	0.015	0.008	0.009	0.017	0.010
Fe	2.599	3.262	3.996	4.164	4.491	6.084	0.786	1.532	2.557	3.245	3.265	4.722	6.064
Mg	4.069	3.466	2.860	2.633	2.295	0.764	6.093	5.275	4.253	3.459	3.460	2.089	0.780
Mn	0.193	0.200	0.095	0.126	0.135	0.085	0.025	0.046	0.066	0.200	0.195	0.128	0.083
Ca	0.125	0.064	0.037	0.018	0.055	0.057	0.089	0.109	0.109	0.087	0.072	0.044	0.063
Fe/(Fe + Mg)	0.390	0.485	0.583	0.613	0.662	0.888	0.114	0.225	0.376	0.484	0.485	0.693	0.886

* Fe_{tot}.
** CaO analysis corrected for actinolite lamellae (see text).
† H_2O analyses determined by manometry, M.D. Dyar, analyst.
‡ F < 0.05 wt% except where a value is given.

cases Al_2O_3 and Na_2O (Table 2). Fe_2O_3 is generally present close to detection-limit levels in cummingtonite and grunerite from many banded iron formations. For example, Klein (1964) reported effectively no Fe_2O_3 in wet chemical analyses of six cummingtonite and grunerite samples, Hafner and Ghose (1971) found Fe^{3+}/Fe_{tot} to be <1% from Mössbauer spectra, and Dyar (1984) and Clowe et al. (1988) confirmed the detection-limit level of Fe_2O_3 in the reference sample 1-K of Klein (1964). Also, Ghose and Weidner (1972) reported no detectable Fe^{3+} in three samples (10141, USNM 118125, and DH7-482) that were heat-treated (like ours) in a reducing atmosphere at 2 kbar. Microprobe analyses detected F (>0.05 wt%) in only one sample (AMNH 27022), and Cl varies from <0.01 to a maximum of 0.14 wt% (Table 2). H_2O contents determined in an H-isotope extraction line (M. D. Dyar, personal communication) for eight of the 13 samples examined gave formula amounts of OH^- ranging from 1.47 to 1.95. At present, we have no good explanation for the apparent deficiency in occupation of the OH sites. All samples in the present study are polysynthetically twinned, and some have microscopic exsolution lamellae of actinolite. Many samples were obtained as pure separates from previous investigators. New samples were crushed, sieved, washed, cleaned in acetic acid, and purified with a Frantz magnetic separator and by final hand-picking.

Heat treatment was performed by sealing 20–80 mg of the sample with 5–10 mg distilled H_2O in annealed $Ag_{60}Pd_{40}$ capsules 2–3 cm long, enclosing three at a time with C and steel filler rods in cold-seal pressure vessels, and raising the vessels to 1 or 2 kbar of CH_4 pressure. Experiment times were selected to optimize equilibrium disorder using the kinetic data of Seifert and Virgo (1974) from anthophyllite as a guide, as follows: 750 °C, 1 d; 700 °C, 2 d; 600 °C, 1 month. Four reversal (i.e., ordering) experiments were conducted at 600 °C for 1 month after an initial 24 h at 750 °C. Comparison of Mössbauer spectra from disordering and ordering experiments (Dyar and Grant, 1993 written communication) verifies that equilibrium was achieved during heat treatment. The temperature was measured with chromel-alumel thermocouples and, considering thermal gradients in the pressure vessels and measurement uncertainty, is believed to be accurate to ±10 °C. Pressure was measured with an Ashcroft (Bourdon) gauge and is probably accurate to within 100 bars. Some experiments at 600 °C with the magnesiocummingtonite samples were conducted without H_2O to preclude the possible formation of talc.

Vessels were quenched inside a coil of air jets. A cooling rate of 7 °C/s over the first 200 °C of cooling was achieved in the experiments at 700 °C and above. Mössbauer spectra of amphiboles taken before and after heat treatment with the C + CH_4 buffer indicate that Fe^{3+} is at or below the limit of detection, which is <1% of Fe_{tot} (M. D. Dyar, 1993 personal communication). In many cases, the samples showed a diminution in average grain size (and probably crystal quality), but no new phases (e.g., talc, magnetite, orthopyroxene) resulted from the heat treatment, even though intrinsic stability conditions for the amphibole were exceeded in some cases.

X-ray diffraction and analysis

The space group of heated crystals was confirmed with Weissenberg X-ray photographs. Ghose and Weidner

TABLE 2.—*Continued*

30a	1c	21a	6b	4b	4a	17c	3b	18a	2b	19a	5c	5b	16a	22f
57.50	56.07	55.26	54.06	54.37	54.11	53.48	51.87	52.45	52.43	51.90	51.13	51.50	50.82	49.55
0.02	0.01	0.01	0.00	0.01	0.01	0.01	0.01	0.00	0.02	0.01	0.01	0.01	0.01	0.01
0.52	0.25	0.09	0.13	0.17	0.14	0.21	0.81	0.02	0.72	0.04	0.32	0.32	0.13	0.15
13.30	19.88	21.19	25.35	26.50	26.95	28.89	31.54	32.17	33.19	34.62	35.46	36.63	38.03	44.22
25.98	20.59	19.44	16.44	15.51	15.64	13.34	11.96	11.90	11.77	10.08	9.88	8.76	7.67	3.26
0.34	0.55	1.44	2.13	1.59	1.62	1.50	0.71	0.58	0.99	0.45	1.10	0.94	0.87	0.61
0.60**	0.65	0.73	0.79	0.53	0.47	0.49	0.39	0.79	0.11	0.60**	0.28	0.25	0.72	0.33
0.12	0.05	0.02	0.08	0.02	0.02	0.01	0.01	0.02	0.08	0.01	0.03	0.02	0.06	0.06
0.01	0.02	0.01	0.01	0.01	0.01	0.01	0.01	0.00	0.02	0.01	0.01	0.01	0.01	0.01
	2.03			1.77	1.77		1.90		1.65	1.59	1.81	1.81	1.41	1.65
							0.12							
0.00	0.00	0.00	0.03	0.08	0.07	0.03	0.00	0.00	0.02	0.03	0.00	0.00	0.08	0.13
0.00	0.00	0.00	0.01	0.02	0.02	0.01	0.05	0.00	0.00	0.01	0.00	0.00	0.02	0.03
98.39	100.10	98.19	99.01	100.54	100.79	97.96	99.28	97.93	101.00	99.33	100.03	100.25	99.79	99.95
					Tetrahedral cations (normalized to sum of 8)									
7.944	7.972	7.990	7.985	7.980	7.984	7.975	7.903	7.998	7.915	7.995	7.961	7.961	7.984	7.981
0.056	0.028	0.010	0.015	0.020	0.016	0.025	0.097	0.002	0.085	0.005	0.039	0.039	0.016	0.019
					M-site cations (normalized to sum of 7)									
0.028	0.014	0.005	0.007	0.010	0.008	0.013	0.049	0.001	0.043	0.002	0.019	0.020	0.008	0.010
1.527	2.396	2.545	3.065	3.282	3.302	3.683	4.054	4.095	4.175	4.502	4.538	4.778	4.970	6.053
5.317	4.423	4.162	3.544	3.424	3.416	3.031	2.740	2.700	2.639	2.337	2.254	2.037	1.787	0.795
0.040	0.067	0.175	0.261	0.199	0.201	0.194	0.092	0.075	0.126	0.059	0.143	0.124	0.115	0.085
0.088	0.100	0.112	0.122	0.084	0.074	0.080	0.064	0.129	0.018	0.100	0.046	0.042	0.121	0.058
0.223	0.351	0.379	0.464	0.489	0.492	0.549	0.597	0.603	0.613	0.658	0.668	0.701	0.736	0.884

(1971a) documented the partial conversion of grunerite to ferrosilite following heating above 775 °C at 500 bars Ar pressure, but no photographic evidence of pyroxene intergrowths was detected in this study. In a few cases, very fine exsolution lamellae of calcic amphibole were detected in electron beam scans from variations in Ca content in microprobe analyses. Individual crystals that had a minimum of twinning were selected by optical examination, although in most cases it was impossible to find crystals completely devoid of twins. Potentially suitable crystals were mounted on a Syntex $P\bar{1}$ four-pole diffractometer and checked for crystal quality using ω scans of diffraction peak shapes. Unit cells of suitable crystals were determined by centering 20–25 peaks with $20° \leq 2\theta \leq 35°$. Intensity data were collected with graphite-monochromated Mo$K\alpha$ radiation and a scan speed of 3°/min for one quadrant of reciprocal space up to $2\theta = 70°$, resulting in a single set of nonequivalent *hkl* reflections. Intensities of three standard reflections were measured after every 100 reflections. Diffraction intensities were corrected for Lorentz polarization and extinction factors. No correction for absorption was applied. Comparison of refinements of the most Fe-rich grunerite examined, 1-K, with and without semiempirical absorption-corrected structure factors yielded indistinguishable results. For example, refined Fe site populations differed by only 0.003, which is $< 1\sigma$.

Following X-ray analysis, the compositions of individual crystals were determined (Table 2) by wavelength-dispersive analysis with a JEOL 733 microprobe using an accelerating potential of 15 kV and a current of 20 nA on brass, natural amphibole and pyroxene standards, and the data reduction procedure of Bence and Albee (1968). For standardization, we used grunerite 1-K of Klein (1964), with $SiO_2 = 49.2\%$ and FeO = 44.7%, on the basis of a microprobe crosscheck with synthetic almandine and ferrosilite (also see analyses of this reference sample listed in Lattard and Evans, 1992), and, for MgO and CaO, we used Campolungo tremolite, with MgO = 24.7% and CaO = 13.46%, on the basis of atomic absorption, ICP analysis, and crosschecks against synthetic diopside and four analyzed natural tremolite samples. Mineral compositions were recalculated to an anhydrous formula unit containing 23 O atoms assuming all Fe as Fe^{2+}, and then recast to total T- and M-site populations (Table 2).

Weighted least-squares refinement was carried out in the space group $C2/m$ or $P2_1/m$ for all reflections with $I \geq 3\sigma$. Compositions were constrained from microprobe analyses using RFINE90, an updated version of RFINE4 (Finger and Prince, 1975), provided by Larry Finger, and scattering factors for neutral atoms, including anomalous dispersion, were employed (Ibers and Hamilton, 1974). Structure factors were weighted according to the formula $w = [\sigma^2(F) + pF^2]^{-1}$, where p was varied empirically to achieve a slope of 1 on a probability plot and generally was equal to 0.02–0.03. Isotropic displacement factors were employed during initial iterations of the refinement; anisotropic displacement factors were introduced following the fourth cycle.

The space group of crystals 1c, 8a, and 11a was originally thought to be $C2/m$, but small irregularities of the refined displacement factors suggested that this assumption was not correct, and more careful examination revealed that the space group of crystals 1c and 11a is $P2_1/m$. Data were then recollected for these crystals, and refinements in the space group $P2_1/m$ resulted in a small improvement of the R factors but little change in the site occupancies. Unfortunately, crystal 8a was lost during the polishing for microprobe analysis. As the site occupancies of crystals 1c and 11a were little affected by the change

TABLE 3. Lattice parameters and refinement statistics

	DH7-482	DH7-484	27022	Lab 510	24159	1-K	45a
a (Å)	9.519(1)	9.520(1)	9.521(1)	9.531(1)	9.547(2)	9.5718(1)	9.4807(8)
b (Å)	18.140(1)	18.185(1)	18.226(1)	18.230(2)	18.272(2)	18.397(2)	17.988(2)
c (Å)	5.3127(5)	5.3192(5)	5.3207(4)	5.3303(6)	5.3315(6)	5.3403(6)	5.2816(5)
β (°)	102.150(3)	102.002(2)	101.913(4)	101.896(5)	101.97(5)	101.867(5)	102.098(3)
V (Å^3)	896.81	900.79	903.42	906.25	909.77	920.28	880.70
Corrected V (Å^3)*	893.89	898.73	902.31	905.34	908.52	919.52	879.19
Space group	$C2/m$	$C2/m$	$C2/m$	$C2/m$	$C2/m$	$C2/m$	$P2_1/m$
Reflections $>3\sigma$	1542	1447	1531	1493	1865	1572	1865
R_w	3.6	7.3	2.8	3.2	5.5	4.1	5.5
R	2.9	6.0	2.2	2.5	4.1	3.0	4.1
	21a	6b	4b	4a	17c	3b	18a
a (Å)	9.5192(6)	9.5328(4)	9.5236(5)	9.5224(5)	9.5335(6)	9.5279(4)	9.5436(4)
b (Å)	18.147(1)	18.1898(9)	18.194(1)	18.197(1)	18.221(1)	18.2451(6)	18.2499(7)
c (Å)	5.3137(3)	5.3208(3)	5.3214(4)	5.3218(4)	5.325(4)	5.3278(2)	5.3273(2)
β (°)	102.019(3)	102.076(3)	102.018(3)	102.016(3)	102.024(3)	101.975(3)	102.054(3)
V (Å^3)	897.81	902.21	901.83	901.97	904.71	906.02	907.4
Corrected V (Å^3)*	895.27	899.19	899.63	899.80	902.70	904.85	905.7
Space group	$C2/m$	$C2/m$	$C2/m$	$C2/m$	$C2/m$	$C2/m$	$C2/m$
Reflections $>3\sigma$	1519	1846	1498	1672	1328	1918	1551
R_w	4.6	3.8	5.5	4.5	3.1	2.3	3.5
R	3.4	2.8	4.2	3.4	2.7	1.8	2.7

Note: $R = \Sigma(|F_o| - |F_c|)/|F_o|$ $R_w = [\Sigma w(|F_o| - |F_c|^2/\Sigma|F_o|^2]^{0.5}$.
* Volume corrected for Mn and Ca impurities (see text).
** Crystal 8a was refined as $C2/m$, though the actual space group is believed to be $P2_1/m$.

in refined space group, we assume that the site occupancies originally determined for crystal 8a continue to be useful, but the other aspects of the refined structure must be considered only as crude estimates.

Although concentrations of minor elements in the crystals studied are small, accurate refinements require the appropriate assignment of Ca, Mn, and Al among the distinct crystallographic sites. These assignments were made as follows: Ca is assumed to occupy only the M4 site. Cummingtonite with >0.6 wt% CaO (≈0.09 atoms Ca pfu) generally coexists with actinolite. Such cummingtonite probably contains submicroscopic exsolution lamellae of actinolite (microscopic in samples 118125, CL1, 7B, DH7-482, and W82-009), in which case the microprobe analysis overestimates the Ca content of what was refined. Fortunately, this uncertainty has a very small effect on the site refinements, as the amount of possible excess Ca is quite small, and the effect of assigning excess Ca to M4 in cummingtonite is to displace approximately equal amounts of Fe and Mg. In the cases of crystals 19a and 30a, the CaO concentration in excess of 0.6% of the analyzed crystal had an effect that was comparable to or greater than other analytical uncertainties. In the case of 19a, the measured microprobe analysis was corrected for a presumed amount of actinolite lamellae; for 30a, the composition was corrected to reflect the composition of other analyzed samples of W82-009, for which significant CaO excesses were avoided.

Al contents range from 0.01 to 0.15 cations pfu; more aluminous cummingtonite samples were excluded at the outset. Al in cummingtonite may occupy the M2 and the T1 sites. A compilation of analyses of Al-bearing, high-temperature, metamorphic and volcanic cummingtonite from the literature revealed that Al substitution is probably best approximated by assuming equal displacement along the edenite ($^{A}Na^{T}Al$, $^{A}\square_{-1}{}^{T}Si_{-1}$) and tschermakite ($^{M}Al^{T}Al$, $^{M}Mg_{-1}{}^{T}Si_{-1}$) vectors. This ratio of ed to tk is higher than the 1:3 ratio in "ideal gedrite" (Robinson et al., 1982), but it is similar to some samples of Na-rich gedrite (Berg, 1985). We chose not to depend on the microprobe determination of Si pfu in the refined crystal ($^{T}Al = 8.0 - Si$) but instead assumed from the foregoing that the small amount of Al present is divided 2:1 between the T1 and the M2 sites. Because there are four T1 and two M2 sites pfu, this results in equal Al-site mole fractions for the T1 and M2 sites. The resulting Al^{M2} pfu in the crystals studied ranges from 0.0024 to 0.0504 (or from 0.12 to 2.5% occupancy of the M2 site).

Na abundances are barely detectable in routine microprobe analysis, reaching only as high as 0.03 pfu in a few instances. In accordance with our assumption regarding Al site-occupancies, we assume that Na occupies the A site as part of the ed substitution and that none is present on M4. During structure refinements, the A site was assumed to be vacant, consistent with the very small charge (it is equivalent in all cases to <0.30 of an electron per unit cell) associated with the possible Na content of this site. Difference-Fourier maps constructed from refinements of the most sodic crystals examined (crystals 2b, 6b, 16a) failed to detect any significant excess charge density at the A site, probably because the small amount of charge is distributed over several of the A subsites (Hawthorne, 1981).

Mn content of examined crystals ranges from 0.02 to 0.27 pfu. Mn is known to concentrate strongly in the M4 site of Mg-, Fe-, and Mn-bearing $C2/m$ and $P2_1/m$ amphiboles, but some Mn is also found in the other M sites (e.g., Bancroft et al., 1967; Papike et al., 1969; Hawthorne and Grundy, 1977; Ghose and Hexiong, 1989). Mn^{2+} is generally thought to concentrate in M4 to a greater extent

TABLE 3.—*Continued*

57d	11a	14a	14g	12a	15b	30a	1c
9.487(1)	9.5048(4)	9.5233(5)	9.5266(5)	9.5369(3)	9.5669(7)	9.490(1)	9.5057(3)
18.035(2)	18.1343(8)	18.1898(8)	18.2117(8)	18.2905(6)	18.397(1)	18.049(2)	18.1187(7)
5.2907(7)	5.3077(2)	5.3223(2)	5.3226(2)	5.3314(1)	5.3416(3)	5.2923(4)	5.3059(3)
102.013(4)	102.009(3)	102.014(3)	101.994(3)	101.917(3)	101.918(3)	102.090(4)	102.031(3)
885.36	894.83	901.77	903.29	909.94	919.86	886.34	893.77
883.80	893.04	899.52	901.30	908.87	919.03	883.69	892.07
$P2_1/m$	$P2_1/m$	$C2/m$	$C2/m$	$C2/m$	$C2/m$	$P2_1/m$	$P2_1/m$
2061	1843	1640	1601	1645	1529	2501	1731
6.6	4.9	3.9	3.7	4.9	4.0	4.8	4.8
5.3	3.6	3.1	2.8	3.6	3.5	3.5	3.6
2b	**19a**	**5c**	**5b**	**16a**	**22f**	**8a**	**9a**
9.5233(3)	9.5507(3)	9.5323(7)	9.5331(5)	9.5568(3)	9.5664(3)	9.5074(4)	9.5431(5)
18.256(5)	18.2869(6)	18.268(2)	18.2746(9)	18.3153(6)	18.4034(6)	18.1334(6)	18.2909(8)
5.331(1)	5.3304(2)	5.3271(6)	5.3278(3)	5.3344(2)	5.3403(2)	5.3081(2)	5.332(2)
101.911(3)	102.030(3)	101.925(3)	101.929(3)	101.962(3)	101.982(3)	101.975(3)	101.949(3)
906.88	910.52	907.60	908.13	913.43	919.70	895.21	910.54
905.95	908.77	906.32	907.02	911.81	918.93		
$C2/m$	$C2/m$	$C2/m$	$C2/m$	$C2/m$	$C2/m$	$C2/m$**	$C2/m$
1778	1712	1821	1724	1691	1476	1561	1513
3.3	4.4	5.0	4.8	2.9	2.6	3.2	3.8
2.4	3.2	4.0	3.5	2.3	2.2	2.7	3.1

than Fe^{2+} (e.g., Ghose and Hexiong, 1989), but there is some evidence that the difference is not large. For example, the site occupancies of a natural, unheated, Mn- and Mg-bearing amphibole are (projected Ca-free) $X_{Mn}^{M4} = 0.950$ and $X_{Mn}^{M1} = 0.150$ (Ghose and Hexiong, 1989), whereas the site occupancies of a natural, unheated, Fe- and Mg-bearing amphibole with comparable Mg content (DH7-482, this study) are $X_{Fe}^{M4} = 0.929$ and $X_{Fe}^{M1} = 0.252$. Mn-Mg and Fe-Mg fractionations, expressed in terms of $\ln K_{14}$ (defined below), are -4.68 and -3.66, respectively. It may be reasonable to assume that Mn site preferences in these amphiboles are comparable in magnitude to those of Fe^{2+}. As a test of the effect of various possible assumptions on the refined site occupancies, X-ray intensity data for each crystal were refined twice, in the first case assuming that Mn is confined to the M4 site, and in the second case grouping Fe and Mn together, using the scattering factors for Fe, and assuming that the Mn-Fe ratio on all the M sites is equal to the macroscopic Mn-Fe ratio of the crystal. It was found that the difference between these two assumptions, in terms of the resulting Fe/(Fe + Mg) ratios of the M sites, was much less than the stated site-occupancy uncertainties. This is largely because of the low Mn content of the amphiboles examined but also because the slightly smaller scattering power of Mn relative to Fe results in marginally lower (Fe + Mn) on the M4 site when some of the Mn is allowed to occupy the M123 sites and therefore slightly greater Mg on the M4 site. We present here only the results of refinements performed with Mn distributed in the same proportions as Fe among all the M sites.

Finding high-quality crystals of cummingtonite-grunerite amphiboles proved to be quite difficult, as many samples are fibrous. In some cases, the crystals used for refinement are of poor quality, and the quality of the refinement is compromised. This problem is particularly acute for Mg-rich varieties, such as KL 14A (crystal 45a); X-ray data were collected on numerous crystals of this sample before one refinement with $R < 10\%$ was achieved.

Refinement statistics are given in Table 3. Site occupancies are given in Table 4, and final positional parameters and equivalent isotropic displacement parameters are given in Table 5.[1] Anisotropic displacement factors are given in Table 6.[1] Difference-Fourier maps revealed no significant charge excesses or deficiencies in refined structures; the largest excess charges amounted to approximately one electron (per 0.25 Å^3) in the vicinity of the presumed H site, but attempts to locate the position of H in the refinements failed to improve refinement statistics or to locate the H position with any reasonable precision.

Quoted 1σ uncertainties for site occupancies in Table 4 only directly include contributions from refinement statistics. In reality, additional uncertainties arise from errors in microprobe analysis and from the assignment of minor components to the M sites. On the basis of duplicate refinements (4a-4b, 5b-5c, and 14a-14g: Table 4) and the consistency of our results on samples equilibrated at 700 °C, we believe that the precision of site occupancies is $\pm 1\%$ (1σ) for homogeneous crystals and $\pm 2\%$ (1σ) for crystals with non-negligible compositional heterogeneity (such as 24159, 12a, 5b, 5c: Table 2).

RESULTS AND DISCUSSION

Space group

Reflections violating the C-centered lattice were detected in cummingtonite crystals with up to 38 mol% Fe/(Fe + Mg). These are considerably more Fe-rich than the most Fe-rich primitive cummingtonite noted by Ghose and Ganguly (0.22: 1982) or by Yakovleva et al. (0.29:

[1] To obtain a copy of Tables 5, 6, and 7, request Document AM-94-562 from the Business Office, 1130 Seventeenth Street, NW, Suite 330, Washington, DC 20036, U.S.A. Please remit $5.00 in advance for the microfiche.

TABLE 4. Occupancies of the M sites

Sample no.	DH7-482	DH7-484	27022	Lab 510	24159	1-K	45a	57d	11a	14a
Heat treatment (°C)	none	none	none	none	none	none	600	600	600	600
					M1					
Fe	0.248(3)	0.370(6)	0.498(2)	0.551(3)	0.603(4)	0.872(3)	0.052(5)	0.110(4)	0.252(4)	0.380(3)
Mg	0.734	0.607	0.490	0.432	0.380	0.116	0.946	0.887	0.741	0.597
Mn	0.018	0.023	0.012	0.017	0.017	0.012	0.002	0.003	0.007	0.023
Fe/(Fe + Mg)	0.252	0.379	0.504	0.561	0.613	0.883	0.052	0.110	0.254	0.389
					M2					
Fe	0.116(3)	0.202(6)	0.319(2)	0.314(3)	0.436(4)	0.781(3)	0.020(5)	0.059(5)	0.161(4)	0.268(3)
Mg	0.868	0.782	0.668	0.673	0.538	0.203	0.975	0.920	0.828	0.711
Mn	0.009	0.012	0.008	0.010	0.013	0.011	0.001	0.002	0.004	0.017
Al	0.007	0.004	0.005	0.003	0.013	0.005	0.004	0.019	0.007	0.004
Fe/(Fe + Mg)	0.118	0.205	0.323	0.318	0.448	0.794	0.020	0.060	0.163	0.274
					M3					
Fe	0.242(4)	0.377(9)	0.501(4)	0.553(4)	0.633(6)	0.897(5)	0.055(7)	0.089(7)	0.216(6)	0.359(5)
Mg	0.740	0.600	0.487	0.430	0.349	0.090	0.943	0.908	0.778	0.619
Mn	0.018	0.023	0.012	0.017	0.018	0.013	0.002	0.003	0.006	0.022
Fe/(Fe + Mg)	0.246	0.386	0.507	0.563	0.645	0.909	0.055	0.090	0.218	0.367
					M4					
Fe	0.814	0.871	0.930	0.940	0.914	0.940	0.293	0.553	0.757	0.795
Mg	0.062	0.044	0.029	0.023	0.033	0.018	0.654	0.375	0.168	0.113
Mn	0.061	0.053	0.022	0.028	0.026	0.013	0.009	0.017	0.020	0.049
Ca	0.063	0.032	0.019	0.009	0.027	0.029	0.044	0.055	0.055	0.043
Fe/(Fe + Mg)	0.929	0.952	0.970	0.976	0.965	0.981	0.309	0.596	0.818	0.876
K_{12}	2.516	2.366	2.126	2.731	1.955	1.953	2.650	1.921	1.754	1.684
K_{13}	1.031	0.971	0.988	0.992	0.875	0.754	0.944	1.257	1.225	1.097
K_{14}	0.026	0.031	0.032	0.031	0.057	0.144	0.124	0.084	0.076	0.090
$-RT \ln K_{12}$ (kJ)							−7.1(20)	−4.7(7)	−4.1(3)	−3.8(1)
$-RT \ln K_{13}$ (kJ)							0.4(12)	−1.6(7)	−1.5(3)	−0.7(2)
$-RT \ln K_{14}$ (kJ)							15.2(8)	18.0(3)	18.7(3)	17.4(2)

TABLE 4.—*Continued*

Sample no.	14g	12a	15b	30a	1c	21a	6b	4b	4a	17c
Heat treatment (°C)	600	600	600	700	700	700	700	700	700	700
					M1					
Fe	0.380(3)	0.629(4)	0.852(3)	0.119(3)	0.240(4)	0.271(4)	0.358(2)	0.387(4)	0.393(3)	0.455(3)
Mg	0.597	0.354	0.136	0.878	0.753	0.710	0.611	0.590	0.583	0.521
Mn	0.023	0.017	0.012	0.003	0.007	0.019	0.031	0.023	0.024	0.024
Fe/(Fe + Mg)	0.389	0.640	0.862	0.119	0.242	0.276	0.370	0.396	0.403	0.466
					M2					
Fe	0.271(3)	0.526(4)	0.805(3)	0.066(3)	0.156(4)	0.182(5)	0.255(3)	0.279(5)	0.286(4)	0.352(3)
Mg	0.709	0.451	0.179	0.907	0.833	0.802	0.720	0.699	0.693	0.625
Mn	0.016	0.014	0.011	0.002	0.004	0.013	0.022	0.017	0.017	0.019
Al	0.004	0.009	0.005	0.025	0.007	0.003	0.003	0.005	0.004	0.004
Fe/(Fe + Mg)	0.276	0.538	0.818	0.068	0.157	0.185	0.262	0.285	0.292	0.361
					M3					
Fe	0.360(5)	0.595(6)	0.844(5)	0.113(5)	0.196(6)	0.240(6)	0.336(4)	0.356(7)	0.365(5)	0.433(5)
Mg	0.619	0.389	0.144	0.884	0.799	0.744	0.635	0.622	0.613	0.544
Mn	0.021	0.016	0.012	0.003	0.005	0.016	0.029	0.022	0.022	0.023
Fe/(Fe + Mg)	0.367	0.605	0.854	0.113	0.197	0.244	0.346	0.364	0.373	0.443
					M4					
Fe	0.801	0.909	0.952	0.520	0.704	0.700	0.750	0.798	0.790	0.818
Mg	0.115	0.044	0.004	0.421	0.226	0.196	0.126	0.112	0.125	0.099
Mn	0.048	0.025	0.013	0.015	0.020	0.048	0.064	0.048	0.048	0.043
Ca	0.036	0.022	0.031	0.044	0.050	0.056	0.060	0.042	0.037	0.040
Fe/(Fe + Mg)	0.874	0.954	0.996	0.553	0.757	0.781	0.856	0.877	0.863	0.892
K_{12}	1.668	1.524	1.394	1.853	1.708	1.680	1.655	1.641	1.636	1.549
K_{13}	1.097	1.162	1.069	1.059	1.304	1.187	1.108	1.143	1.133	1.097
K_{14}	0.091	0.086	0.026	0.109	0.102	0.107	0.099	0.092	0.107	0.106
$-RT \ln K_{12}$ (kJ)	−3.7(1)	−3.1(2)	−2.3(2)	−5.0(4)	−4.3(3)	−4.2(3)	−4.1(1)	−4.0(2)	−4.0(2)	−3.5(1)
$-RT \ln K_{13}$ (kJ)	−0.7(2)	−1.1(2)	−0.5(3)	−0.5(5)	−2.1(4)	−1.4(3)	−0.8(2)	−1.1(3)	−1.0(2)	−0.7(2)
$-RT \ln K_{14}$ (kJ)	17.4(2)	17.8(7)	26(6)	17.9(3)	18.4(3)	18.1(3)	18.7(2)	19.3(4)	18.0(3)	18.2(3)

1978) but similar to a $P2_1/m$ cummingtonite (0.36) described by Robinson and Jaffe (1969) and less Fe-rich than primitive cummingtonite (0.44, 0.45) from the Ruby Mountains, Montana, described by Ross et al. (1969) and Immega and Klein (1976).

Unit cells

Lattice parameters determined in this study (Table 3) are compared with previous determinations in Figure 1. The a and b parameters vary linearly with macroscopic

TABLE 4.—*Continued*

Sample no.	3b	18a	2b	19a	5c	5b	16a	22f	8a	9a
Heat treatment (°C)	700	700	700	700	700	700	700	700	750	750
					M1					
Fe	0.506(2)	0.527(3)	0.537(2)	0.593(3)	0.594(3)	0.636(4)	0.678(2)	0.853(2)	0.264(3)	0.626(3)
Mg	0.482	0.463	0.447	0.399	0.387	0.347	0.306	0.135	0.729	0.357
Mn	0.012	0.010	0.016	0.008	0.019	0.017	0.016	0.012	0.007	0.017
Fe/(Fe + Mg)	0.512	0.532	0.546	0.598	0.606	0.647	0.689	0.863	0.266	0.637
					M2					
Fe	0.409(2)	0.429(3)	0.420(3)	0.493(3)	0.492(3)	0.537(4)	0.592(2)	0.810(3)	0.180(3)	0.533(3)
Mg	0.558	0.562	0.546	0.500	0.483	0.439	0.390	0.174	0.808	0.444
Mn	0.009	0.008	0.013	0.006	0.015	0.014	0.014	0.011	0.005	0.014
Al	0.024	0.001	0.021	0.001	0.010	0.010	0.004	0.005	0.007	0.009
Fe/(Fe + Mg)	0.423	0.433	0.435	0.496	0.504	0.550	0.603	0.823	0.182	0.545
					M3					
Fe	0.493(3)	0.502(5)	0.506(4)	0.580(5)	0.594(5)	0.620(6)	0.665(4)	0.848(4)	0.245(5)	0.604(5)
Mg	0.496	0.489	0.479	0.412	0.387	0.364	0.320	0.140	0.749	0.380
Mn	0.011	0.009	0.015	0.008	0.019	0.016	0.015	0.012	0.006	0.016
Fe/(Fe + Mg)	0.498	0.506	0.514	0.585	0.606	0.630	0.675	0.858	0.246	0.614
					M4					
Fe	0.866	0.841	0.877	0.876	0.887	0.904	0.882	0.939	0.711	0.901
Mg	0.082	0.080	0.087	0.063	0.062	0.051	0.038	0.019	0.215	0.053
Mn	0.020	0.015	0.027	0.011	0.028	0.024	0.020	0.013	0.019	0.024
Ca	0.032	0.064	0.009	0.050	0.023	0.021	0.060	0.029	0.055	0.022
Fe/(Fe + Mg)	0.914	0.913	0.910	0.933	0.935	0.947	0.959	0.980	0.768	0.944
K_{12}	1.435	1.492	1.560	1.509	1.509	1.499	1.460	1.358	1.624	1.462
K_{13}	1.058	1.110	1.137	1.055	1.000	1.077	1.067	1.043	1.109	1.104
K_{14}	0.099	0.108	0.119	0.107	0.107	0.103	0.096	0.128	0.109	0.103
$-RT \ln K_{12}$ (kJ)	−2.9(1)	−3.2(1)	−3.6(1)	−3.3(1)	−3.3(1)	−3.3(2)	−3.1(1)	−2.5(2)	−4.1(2)	−3.2(2)
$-RT \ln K_{13}$ (kJ)	−0.5(1)	−0.8(2)	−1.0(1)	−0.4(2)	−0.0(2)	−0.6(3)	−0.5(2)	−0.3(3)	−0.9(3)	−0.8(2)
$-RT \ln K_{14}$ (kJ)	18.7(2)	18.0(6)	17.2(3)	18.1(5)	18.0(5)	18.4(7)	19.0(5)	16.6(12)	18.8(2)	19.3(6)

Fe/(Fe + Mg), but the c parameter is slightly concave downward (Fig. 1). The percentage change in b is twice as great as that for a and c. This indicates that the chemical expansion in ferromagnesian amphibole is accommodated by a significantly different mechanism than is thermal expansion, for which a and b expand at approximately the same rate while c expands at a considerably smaller rate (Sueno et al., 1972). Variations of β with composition are not much greater than analytical uncertainty, but there is a weak correlation of increasing β with decreasing Fe/(Fe + Mg). There are no discernible systematic differences between the unit-cell dimensions or cell volumes of heated (partially disordered) cummingtonite and unheated (more ordered) cummingtonite of this work or of previous studies in Figure 1. The effect of ordering on unit-cell dimensions must therefore be small, which implies that ordering in cummingtonite should not be sensitive to pressure.

Crystal structures

Mean bond lengths, $\langle M_i\text{-O}\rangle$, of the sites in the octahedral strip of the refined amphiboles correlate with the mean ionic radius, $\langle r_{M_i}\rangle$, of the site occupants (Fig. 2), in general agreement with the trends first outlined for $C2/m$ amphiboles by Hawthorne (1981). In detail, the equations derived by Hawthorne (1981) progressively underestimate ⟨M1-O⟩, ⟨M2-O⟩, and ⟨M3-O⟩ of Al-poor amphiboles with increasing Fe and Mn content (Fig. 2). This is presumably because the regressions of Hawthorne (1981) were derived from amphiboles with more varied occupation of the M2, O3, and A sites than those in this study. For the near-binary ferromagnesian amphiboles from the present work, the relationships between mean ionic radii and average bond lengths for the octahedral sites are given (in Å) by

$$\langle \text{M1-O}\rangle = 1.359 + 1.006\langle r_{M1}\rangle, \quad R^2 = 0.97 \quad (1a)$$

$$\langle \text{M2-O}\rangle = 1.365 + 0.999\langle r_{M2}\rangle, \quad R^2 = 0.97 \quad (1b)$$

$$\langle \text{M3-O}\rangle = 1.358 + 0.996\langle r_{M3}\rangle, \quad R^2 = 0.90. \quad (1c)$$

For a given mean ionic radius, the M1 and M2 sites of ferromagnesian clinoamphibole have indistinguishable mean bond lengths, but the mean length of the M3-O bonds is approximately 0.05 Å shorter than that of the M1-O and M2-O bonds (Fig. 2). This relationship is evident in refinements of other Al-poor clinoamphibole structures, including both hydroxy- and fluor-amphiboles (e.g., Fischer, 1966; Finger, 1969; Papike et al., 1969; Cameron and Gibbs, 1973; Mitchell et al., 1971; Ghose and Ganguly, 1982; Ghose and Hexiong, 1989; Phillips et al., 1991), but is the opposite of that interpreted for a series of sodic-calcic and alkali amphiboles by Ungaretti et al. (1981). Presumably the smaller M3 site observed for Al-poor amphiboles does not persist in more aluminous amphiboles, owing to the inverse relationship noted by Hawthorne (1981) between M3 site bond lengths and the mean bond length of the M2 site. The smaller intrinsic dimension of the M3 site is apparently not sufficient to generate a significant site preference between M1 and M3. Preference of Mg for M2 over M1 and M3 must be attributed to factors other than site dimensions, such as bonding effects and proximity to the M4 site (Hawthorne, 1981).

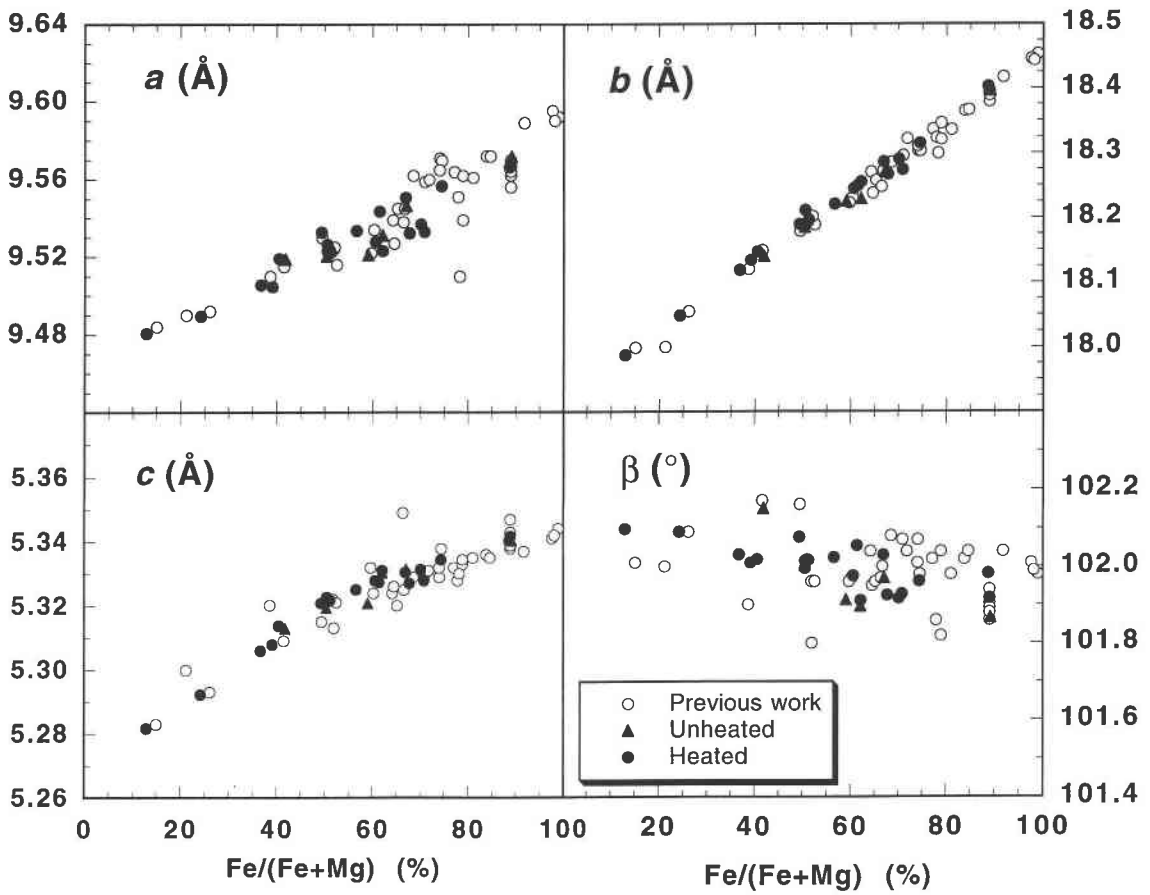

Fig. 1. Lattice parameters for heated and natural cummingtonite. Data from previous work on natural cummingtonite from Kisch (1969), Klein and Waldbaum (1967), Kamineni (1973), Rice et al. (1974), Hawthorne et al. (1980), Clowe et al. (1988), Lattard and Evans (1992), and Zhang et al. (1992).

Mean M4-O bond distances, $^{[6]}\langle$M4-O$\rangle$, and $^{[8]}\langle$M4-O$\rangle$, correlate poorly with $\langle r_{M4}\rangle$ but increase slightly with macroscopic Fe/(Fe + Mg), primarily owing to large changes in the longer M4-O5 and M4-O6 distances (Table 7[1]). The M4-O4 bond distance actually decreases with increasing Fe/(Fe + Mg), which is consistent with the inference that this bond has considerable covalent character (Ghose and Ganguly, 1982). The better correlation of $\langle$M4-O$\rangle$ with bulk composition than with $\langle r_{M4}\rangle$ suggests that the dimensions of the M4 cavity in cummingtonite-grunerite amphiboles are not controlled by size of the occupying cations but are instead controlled by the overall dimensions of the amphibole lattice, which in turn are most strongly influenced by the mean ionic radii of the constituents of the octahedral strip.

Within the octahedral strip, the M3 site shows the greatest angular deviation from a perfect octahedron, and the M1 and M2 sites show lesser and approximately similar deviations (Fig. 3). Angular distortions of the M2 and M3 sites are correlated with bulk composition, as the M2 and M3 sites become more regular with increasing Mg content, but those of the M1 site are insensitive to composition.

Mean tetrahedral bond lengths of the T1 sites, $\langle$T1-O$\rangle$, range from 1.616 to 1.622; mean tetrahedral bond lengths of the T2 sites, $\langle$T2-O$\rangle$, range from 1.625 to 1.630 (Table 7). Mean T1 and T2 bond lengths do not vary with macroscopic Fe/(Fe + Mg). Bond angles for the T1 site are nearly those of an ideal tetrahedron, but those of the T2 site deviate slightly from the ideal 109.47°.

Ordering

Ordering of Fe and Mg in an amphibole of composition $(Fe,Mg)_7Si_8O_{22}(OH)_2$ may be analyzed in terms of three independent ordering reactions:

$$\tfrac{1}{2}Mg_2^{M1} + \tfrac{1}{2}Fe_2^{M2} \leftrightarrow \tfrac{1}{2}Mg_2^{M2} + \tfrac{1}{2}Fe_2^{M1} \quad (2)$$

$$\tfrac{1}{2}Mg_2^{M1} + Fe^{M3} \leftrightarrow Mg^{M3} + \tfrac{1}{2}Fe_2^{M1} \quad (3)$$

$$\tfrac{1}{2}Mg_2^{M1} + \tfrac{1}{2}Fe_2^{M4} \leftrightarrow \tfrac{1}{2}Mg_2^{M4} + \tfrac{1}{2}Fe_2^{M1}. \quad (4)$$

These reactions are written with fractions to emphasize the difference in multiplicities of the M sites. When the ordering reaction is written in the conventional manner,

$$Mg^{M1} + Fe^{M3} \leftrightarrow Mg^{M3} + Fe^{M1} \quad (5)$$

it cannot simultaneously conserve mass and represent an exchange between sites occupied only by Mg or Fe, and

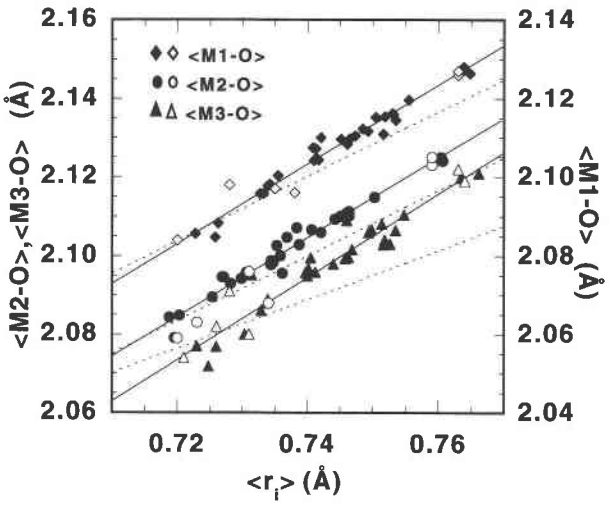

Fig. 2. Mean M-O bond lengths of M1, M2, and M3 sites vs. mean ionic radius of site occupants. Data points and regression lines for M1 are displaced upward by 0.02 Å and correspond to the scale on the right of the diagram; the data points and regression lines for M2 and M3 correspond to the scale on the left of the diagram. Without this displacement, the trends for M1 and M2 would not be distinguishable. Solid symbols are from this work, open symbols are previously published Fe-, Mg-, and Mn-bearing clinoamphibole structure refinements from Fischer (1966), Finger (1969), Papike et al. (1969), Ghose and Ganguly (1982), Ghose and Hexiong (1989), and Phillips et al. (1991). Dashed lines are relationships proposed by Hawthorne (1981) for *C2/m* amphibole of widely varying composition. [Hawthorne's equation for ⟨M3-O⟩ depends partly on $\langle r_{M2} \rangle$. The line for ⟨M3-O⟩ is calculated by substituting the correlation between $\langle r_{M2} \rangle$ and $\langle r_{M3} \rangle$ for the structures in this study ($\langle r_{M2} \rangle = 0.0527 + 0.9371 \cdot \langle r_{M3} \rangle$; $R^2 = 0.92$) into Hawthorne's equation.] Solid lines are the least-squares regression of data from the present work given in Eq. 1a, 1b, and 1c in the text. Ionic radii are from Shannon and Prewitt (1969).

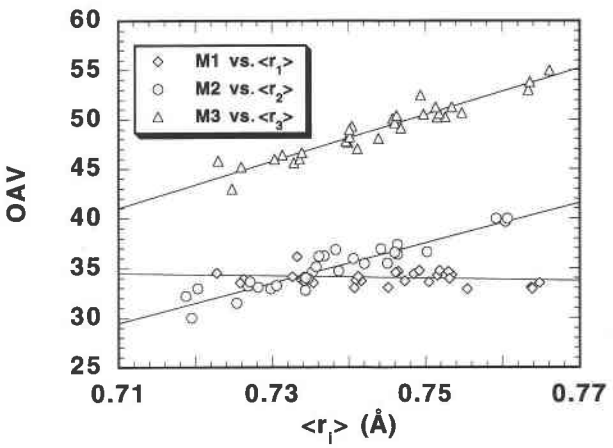

Fig. 3. Octahedral angle variance (OAV) of M1, M2, and M3 sites for cummingtonite; OAV = $\Sigma_{i=1}^{n} (\theta_i - 90)^2/11$.

therefore Reaction 5 cannot be related easily to equations governing the energy of ordering. For similar reasons, attempts to extract mixing properties of amphiboles by analysis of reactions of the form

$$Mg^{M123} + Fe^{M4} \leftrightarrow Mg^{M4} + Fe^{M123} \quad (6)$$

(e.g., Hafner and Ghose, 1971) are inappropriate, as they do not account for the effect of differing site multiplicities on the site-specific activities.

Free-energy changes associated with Reactions 2–4 cannot be determined without considering the possible effects of nonideal mixing within the individual sites. This exercise will be left to a future study, but it is still possible to consider the ideal contribution to the ordering reaction between sites i and j, $-RT \ln K_{ij}$, where at equilibrium

$$\Delta\overline{G}_{ij}^{\text{reaction}} = \Delta\overline{G}_{ij}^{0} + RT \ln K_{ij} + \Delta\overline{G}_{ij}^{XS} = 0 \quad (7)$$

and

$$K_{ij} = \frac{X_{Fe}^{M_i} X_{Mg}^{M_j}}{X_{Mg}^{M_i} X_{Fe}^{M_j}}. \quad (8)$$

In Equation 7, $\Delta\overline{G}_{ij}^{0}$ is the difference in free energy between the hypothetical, pure, ordered amphibole endmembers, and $\Delta\overline{G}_{ij}^{XS}$ is the difference in excess free energy associated with nonideal mixing on individual sites. $X_{Fe}^{M_i}$ is the mole fraction of Fe on the M_i site, which, for the purposes of this exercise, is calculated by projection to the Mg-Fe binary.

There is no discernible temperature dependence to the measured ideal free energies of ordering over the temperature range 600–750 °C (Fig. 4). Of the independent reactions (Reactions 2–4), the most pronounced ideal ordering energy observed is $-RT \ln K_{14}$. The energy of this reaction appears to be independent of composition, and the weighted mean value of $-RT \ln K_{14}$ is 18.2 ± 0.3 kJ (1σ). Of 24 determinations, 23 are within the analytical uncertainty (2σ) of this range. The sole exception is crystal 45a, for which $-RT \ln K_{14} = 15.2 \pm 0.8$ (1σ) (Table 4). This crystal is the most Mg-rich examined, which may indicate that $-RT \ln K_{14}$ is slightly smaller for very Mg-rich cummingtonite than for more Fe-rich compositions, an observation supported by the available Mössbauer data (see below).

Fe weakly prefers the M1 site relative to the M3 site. Measured ideal ordering energies range from −2.0 to 0.4 kJ and yield a weighted mean of −0.7 ± 0.2 kJ (1σ) (Fig. 4). There is some indication of a minimum in $-RT \ln K_{13}$ near Fe/(Fe + Mg) = 0.4 (Fig. 4), but a nonconstant fit to this parameter is not statistically justified.

Mg concentrates in M2 relative to M1, but the magnitude of this effect decreases linearly with increasing bulk Fe content such that

$$-RT \ln K_{12}(\text{kJ}) = -5.64 + 3.65[\text{Fe}/(\text{Fe} + \text{Mg})] \quad (1\sigma = 0.3). \quad (9)$$

This compositional variation does not appear to be related to the effects of next nearest neighbors on the M4 site. Such a mechanism would be expected to lead to a

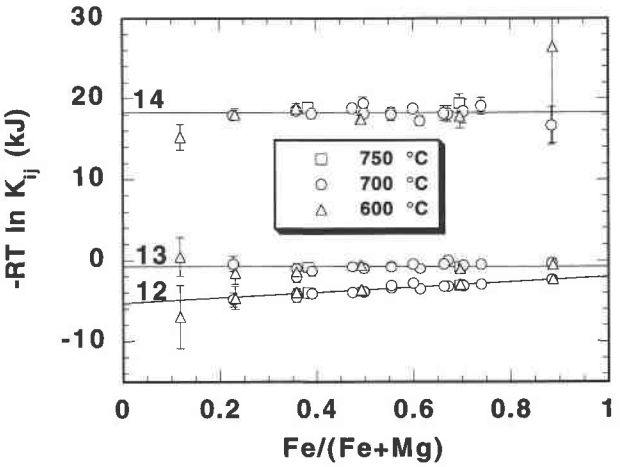

Fig. 4. Ideal ordering energies between M sites for heated cummingtonite. Numbers *ij* beside each line indicate the ordering reaction K_{ij} of the particular line and associated data points. Error bars are 2σ. The magnitude of errors in K_{ij} increases geometrically as Fe/(Fe + Mg) approaches zero or one, as the site mole fractions of Mg or Fe become small relative to their analytical uncertainties.

kink in $-RT \ln K_{12}$ vs. macroscopic Fe/(Fe + Mg) near macroscopic Fe/(Fe + Mg) = 0.3, where X_{Fe}^{M4} ceases to change rapidly with increasing Fe content, but no such kink is observed (Fig. 4). The compositional variation of $-RT \ln K_{12}$ may instead be related to the increasing selection between Mg and Fe on the M2 site caused by shrinkage of the surrounding lattice. From the point of view of mineral thermodynamics, the increase in ordering with increasing Mg content implies that the free energy of the reciprocal reaction

$$Mg_2^{M4}Mg_2^{M2}Mg_3^{M13} + Fe_2^{M4}Fe_2^{M2}Fe_3^{M13} \Leftrightarrow Mg_2^{M4}Fe_2^{M2}Mg_3^{M13} + Fe_2^{M4}Mg_2^{M2}Fe_3^{M13} \quad (10)$$

is positive.

The foregoing discussion is based on the assumption that all of the Fe in the amphiboles examined is Fe^{2+}. Because Fe^{3+} concentrates strongly in the M2 site (Hawthorne and Grundy, 1978), ignoring any Fe^{3+} present would cause insufficiently negative estimates of $-RT \ln K_{12}$. For the hypothetical case in which 1% of Fe_{tot} is Fe^{3+} occupying the M2 site, there is a negligible effect on $-RT \ln K_{12}$ for Fe-rich compositions. With decreasing macroscopic Fe/(Fe + Mg) content, such a proportion of Fe^{3+} would become increasingly important because of the small relative abundance of Fe on the M2 sites at low macroscopic Fe^{2+} concentrations. For the most Mg-rich compositions, 1% Fe_{tot}^{3+} could decrease $-RT \ln K_{12}$ by 1–2 kJ. In fact, Mössbauer spectra show that the heat-treated samples used in this study contain as much as 1% Fe^{3+}/Fe_{tot} in only two cases: 24159 heat-treated at 700 °C (5b, 5c) and DH7-484 heat-treated at 600 °C (14a, 14g) (M. D. Dyar, 1993 written communication). The effect of Fe^{3+} is insignificant in the former case, as the sample is Fe-rich, but in the latter case it results in an increase in the ideal ordering energy of about 0.5 kJ.

The effect of temperature on order-disorder is best examined using Roozeboom plots (Fig. 5). As expected, M1-M2 and M1-M4 ordering is more pronounced in unheated crystals than in those that were heat-treated. Ordering between the M1 and M3 sites is essentially absent in the unheated crystals, but Fe may have a slight preference for M3, which is the opposite of the preference observed in heated samples (Fig. 5). As noted above, the ordering energies extracted in the present analysis are only the ideal contributions to the free energies of the ordering reactions. The extracted values of $-RT \ln K_{12}$ and $-RT \ln K_{14}$ cannot be used alone to predict site occupancies over a large temperature interval, as possible site nonidealities at lower temperature could become significant; such an analysis will be possible following a more complete thermodynamic treatment.

Molar volumes of magnesiocummingtonite, grunerite, and anthophyllite

Unit-cell determinations from this study may be combined with previously measured cell volumes (see captions to Figs. 1 and 6 for references) to provide refined estimates of the molar volumes of end-member magnesiocummingtonite and grunerite for incorporation in thermodynamic data bases. The use of natural compositions, however, requires that corrections be made for the effects of Mn and Ca on the cell volume. We have corrected for Mn by adopting an extrapolated cell volume of 946 Å^3 for fictive $Mn_7Si_8O_{22}(OH)_2$ (Maresch and Czank, 1988) and assuming a linear composition-volume relationship. Calculation of a correction for the effect of Ca on unit-cell volume can be made by averaging the volume of the fictive $Ca_7Si_8O_{22}(OH)_2$ end-member calculated by projecting (1) from $Mg_7Si_8O_{22}(OH)_2$ through $Ca_2Mg_5Si_8O_{22}(OH)_2$ and (2) from $Fe_7Si_8O_{22}(OH)_2$ through $Ca_2Fe_5Si_8O_{22}(OH)_2$. This process is itself not without uncertainty, as it requires estimates for the molar volumes of $Ca_2Mg_5Si_8O_{22}(OH)_2$ and $Ca_2Fe_5Si_8O_{22}(OH)_2$, and the necessary data base includes synthetic material poorly characterized compositionally. The resulting estimate for the volume of $Ca_7Si_8O_{22}(OH)_2$ is 980 Å^3. Given the small amounts of Ca and Mn in the cummingtonite compositions examined, we believe that linear corrections are justified.

Cell volumes for ferromagnesian amphiboles projected to be free of Mn and Ca are shown in Figure 6. Linear least-squares regression of the corrected cell volumes of cummingtonite extrapolate to end-member cell volumes for grunerite and magnesiocummingtonite of 924.5 ± 0.3 and 874.4 ± 0.4 Å^3 (1σ), respectively. Statistical tests indicate that a fit other than linear is not justified.

The trend of anthophyllite (half-cell) volumes is indistinguishable from that of cummingtonite (Fig. 6), which implies that the change in volume associated with the *C2/m* to *Pnma* phase transition in ferromagnesian amphibole is probably <0.5 Å^3 on a monoclinic unit-cell

basis. Synthetic anthophyllite tends to have a larger cell volume than natural ferromagnesian amphibole, particularly in the Mg-rich region (Fig. 6). Chernosky and Autio (1979) reported that their synthetic anthophyllite contained up to 10% by volume of triple-chain silicate. However, the excessive volumes appear to be greater than can be ascribed to peak broadening caused by the presence of chain-width errors, according to the cell dimensions of likely polysomes given by Veblen and Burnham (1978). Maresch and Czank (1988) used HRTEM images to demonstrate that the excessive cell volume of synthetic Mn-bearing magnesioanthophyllite correlates with a high density of (100) chain-stacking faults (also found in natural anthophyllite: Smelik and Veblen, 1993). Although the natural anthophyllite sample 7.3.71.10 was reported to contain approximately 5% wide-chain material (Krupka et al., 1985), it does not have an unusually large cell volume. For these reasons, synthetic amphiboles were not used in the least-squares fits. A fit to the Mg end-member through all the natural cummingtonite and anthophyllite samples (predominantly anthophyllite at the Mg-rich end) extrapolates to 873.9 ± 0.3 Å^3, a value that is not statistically distinguishable from the fit to cummingtonite alone. Our volume for end-member anthophyllite is smaller than that adopted in the thermodynamic data bases of Berman (1988: V = 882.1 Å^3) and Holland and Powell (1990: V = 881.4 Å^3), values based on the volume of a carefully prepared synthetic anthophyllite (anthophyllite III: Chernosky et al., 1985, their Table 3). Our cummingtonite-grunerite end-member cell volumes translate into molar volumes of 26.33 and 27.84 J/bar, respectively, for $Mg_7Si_8O_{22}(OH)_2$ and $Fe_7Si_8O_{22}(OH)_2$.

Comparison with results from Mössbauer spectroscopy

To facilitate comparison with Mössbauer data, it is necessary to consider ordering between M4 and a combined M123 site. In this case, the exchange reaction is

$$^1/_5\,Mg_5^{M123} + {}^1/_2\,Fe_2^{M4} \leftrightarrow {}^1/_2\,Mg_2^{M4} + {}^1/_5\,Fe_5^{M123} \quad (11)$$

and the ideal contribution to the free energy of reaction is

$$-RT\ln K_{123/4} = -RT\ln\frac{X_{Fe}^{M123}X_{Mg}^{M4}}{X_{Mg}^{M123}X_{Fe}^{M4}}. \quad (12)$$

Because Mg site populations are determined from Mössbauer spectroscopy by difference, it is important to account appropriately for other cations occupying M sites, such as Mn, Ca, and Al. This is especially true for Fe-rich grunerite, where the fraction of M4 occupied by Mg is comparable in magnitude to that of Ca and Mn (Table 4). The relative uncertainty in Mg on the M4 site therefore becomes magnified with increasing sample Fe content. In X-ray refinement, the Mg content of sites is not obtained by difference; instead, uncertainty in the assignment of Mn mainly affects the Fe content, and the effect on Fe/(Fe + Mg) ratios is therefore small.

The treatment of Mn and Ca in previous studies has not been uniform. For example, Bancroft et al. (1967)

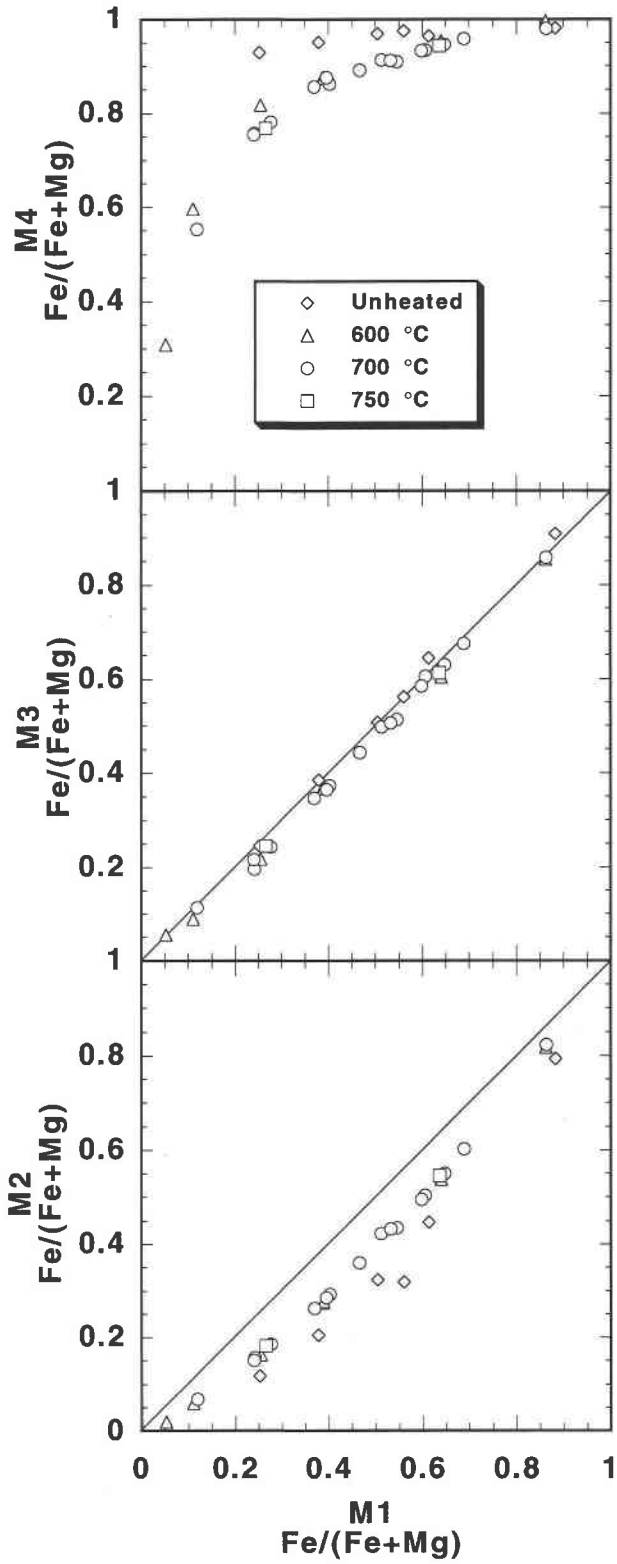

Fig. 5. Roozeboom plots of site occupancies of heated and unheated cummingtonite.

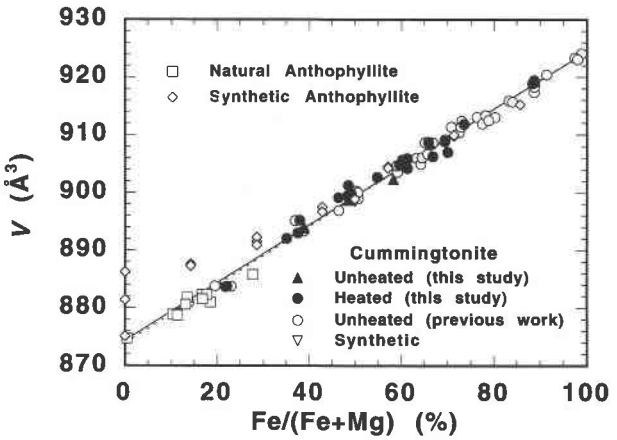

Fig. 6. Volumes of ferromagnesian amphiboles projected to the $(Fe,Mg)_7Si_8O_{22}(OH)_2$ binary by the method explained in the text. The solid straight line is a least-squares fit to cummingtonite volumes and gives intercepts of 874.4 ± 0.4 (1σ) at pure magnesiocummingtonite and 924.5 ± 0.3 Å at pure grunerite. The dashed line is a least-squares fit to both natural ortho- and clinoamphibole volumes, with intercepts at 873.9 ± 0.3 Å at pure $Mg_7Si_8O_{22}(OH)_2$ and 924.7 ± 0.2 Å at pure $Fe_7Si_8O_{22}(OH)_2$. Data for natural cummingtonite other than from this study are from sources listed in the caption in Fig. 1. The synthetic cummingtonite datum is from Cameron (1975). Natural anthophyllite data are from Lindemann (1964), Seifert (1978), Veblen and Burnham (1978), Krupka et al. (1985), Walitzi et al. (1989), and Yang and Evans (unpublished data). Synthetic anthophyllite data are from Greenwood (1963), Chernosky et al. (1985), and Popp et al. (1977).

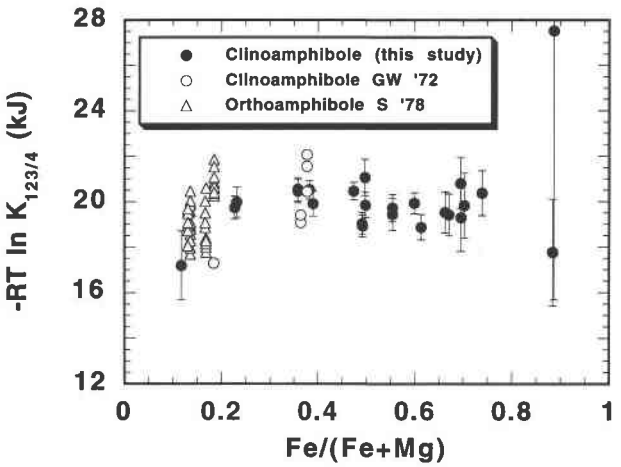

Fig. 7. The comparison of ideal site-preference energies between M4 and M123 for heated ferromagnesian amphibole measured by X-ray diffraction (this study) and Mössbauer spectroscopy. Mössbauer data: GW '72 = heated cummingtonite, Ghose and Weidner (1972); S '78 = heated anthophyllite, Seifert (1978).

and Seifert (1978) assigned all Ca and Mn to the M4 site, whereas Hafner and Ghose (1971) and Ghose and Weidner (1972) distributed Mn and Ca equally among all the M sites. To permit comparison with the present work, we have projected the site Fe/(Fe + Mg) ratios of the Mössbauer determinations from these studies using the same assumptions as used here for the X-ray data; Ca is confined to M4, and Mn is distributed between the M sites in the same proportions as Fe. The importance of this projection for the interpretation of the Mössbauer data is increased by the high Mn content of many of the samples studied by Mössbauer spectroscopy.

Comparison of site-occupancy determinations by X-ray diffraction and Mössbauer spectroscopy must, as noted earlier, address the possibility of systematic differences between the results of the two techniques. Fe fractionations in reequilibrated (heated) and unheated cummingtonite as determined on the same samples by X-ray refinement (this study) and Mössbauer spectroscopy (Dyar and Grant, 1993 written communication) are similar, but the degree of ordering inferred from X-ray diffraction is slightly greater than that deduced from Mössbauer spectra. Similar discrepancies have been noted for orthopyroxene (Domeneghetti and Steffen, 1992; Skogby et al., 1992). One possible factor that might contribute to such discrepancies would be possible differences between the M sites in recoilless-free fractions, as has been empirically deduced for grunerite by Bancroft et al. (1967).

Ghose and Weidner (1972) used Mössbauer spectroscopy to examine Fe site populations in three cummingtonite samples heat-treated at 500, 600, and 700 °C. When projected in the manner described above, the agreement between site occupancies determined by Ghose and Weidner (1972) and the present results is very satisfactory (Fig. 7). Although Ghose and Weidner (1971b) also used Mössbauer spectroscopy to examine ordering in more Fe-rich amphiboles, results have only been presented graphically, and it is not possible to make the appropriate projection to meaningfully compare these data with the present results.

Fe-Mg ordering in anthophyllite and its temperature dependence as determined by Mössbauer spectroscopy (Seifert, 1978) are similar to those determined for cummingtonite in this study (Fig. 7). The similarity of octahedral site ordering in cummingtonite and anthophyllite implies that the *C2/m* to *Pnma* phase transition has little effect on the relative energetics of the M4 and M123 sites. We would anticipate the relative stability of Fe vs. Mg within the M123 sites to be unaffected by this change in symmetry, as the geometries of these site environments are little affected by the transition. The M4 sites of anthophyllite and cummingtonite have different point symmetries, however, and it is somewhat less expected that there should be similar site preference energies for these sites, relative to M123.

The trend of ordering energies at the Mg-rich end of Figure 7 suggests that $-RT \ln K_{123/4}$ is composition-dependent for Mg-rich cummingtonite and anthophyllite. The region of apparently variable $-RT \ln K_{123/4}$ is found for bulk compositions with Fe/(Fe + Mg) < ~0.3. It is in this compositional range that the M4 site population changes rapidly; above Fe/(Fe + Mg) = 0.3, the M4 site

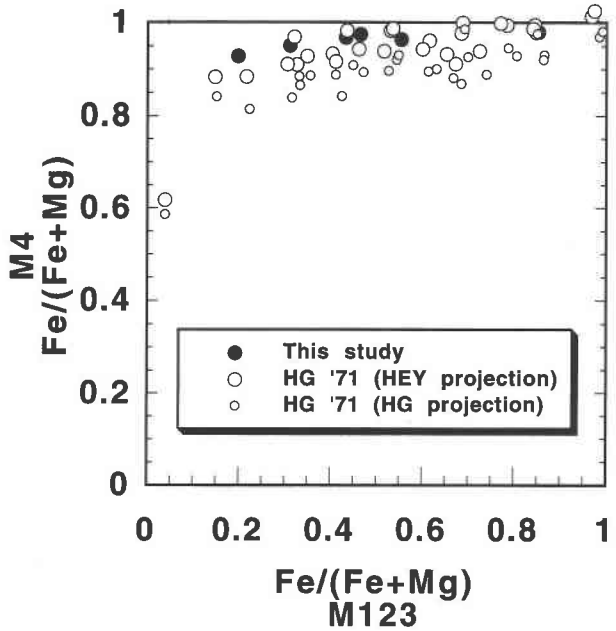

Fig. 8. The comparison of M4 and M123 site occupancies for unheated ferromagnesian amphibole measured by X-ray diffraction (this study) and Mössbauer spectroscopy (Hafner and Ghose, 1971). Points labeled HG are as calculated by Hafner and Ghose (1971); those labeled HEY are calculated by assuming that Ca is confined to M4 and Mn is distributed like Fe^{2+}, as explained in the text.

is largely occupied by Fe. It would seem that the occupancy of the M4 site affects the energetics of the Fe or Mg cations residing on M4 such that Mg is increasingly stabilized in M4 relative to Fe with increasing occupancy of Mg. These effects could possibly be caused by the positional disorder of Mg on M4 or by increasing local strains associated with Fe substitution on M4 as the structure shrinks for more Mg-rich bulk compositions. We are currently conducting an X-ray study of ordering in Mg-rich anthophyllite that should shed additional light on ordering behavior in the Mg-rich limit.

Hafner and Ghose (1971) used Mössbauer spectroscopy to examine ordering in a large number of unheated natural cummingtonite samples. When projected using the conventions described above, the site occupancies of these samples are quite similar to those determined for unheated cummingtonite samples by X-ray diffraction in this study (Fig. 8). The Mössbauer spectra for unheated cummingtonite indicate slightly less order than the X-ray diffraction determinations, and this may again be the result of a small systematic difference between techniques.

As is evident in Figure 8, when projected using the methods described here, the site occupancies of Hafner and Ghose (1971) are significantly different from those projected by the method used by Hafner and Ghose. Consideration of the latter site occupancies leads to the rather surprising inference that unheated grunerite is less ordered than heated grunerite (Figs. 1–3 in Ghose, 1981). Ghose (1990) has suggested that long-range ordering in Fe-rich grunerite may be inhibited by magnetic ordering phenomena up to temperatures of 700 °C. This hypothesis is not supported by site occupancies determined from the X-ray diffraction of heated and unheated grunerite, nor is it supported by the Mössbauer data when these are projected by the methods described in this work.

Acknowledgments

We thank the following individuals and organizations for providing us with samples: S. Ghose, C. Klein, S.E. Hoffman, the U.S. National Museum, the American Museum of Natural History, the Harvard University Mineralogical Museum, and the Royal Ontario Museum. U. Mäder, J.V. Ross, D. McPhail, R. Rodway, and D.M. Kerrick kindly provided assistance to B.W.E. in laboratory work at U.B.C., Vancouver. At the University of Washington, D. McDougall performed the delicate task of expertly polishing fragile single crystals, and S.M. Kuehner gave generous help with electron microprobe analysis. M.D. Dyar and C. Grant are thanked for sharing H_2O analyses and results of Mössbauer spectroscopy in advance of publication. We are also grateful to W. Maresch for sharing unpublished tirodite cell dimensions. Larry Finger kindly supplied an updated version of RFINE. We thank S. Ghose for permission to use the facilities in his X-ray crystallography laboratory. This work was supported by NSF grant EAR-9104714 to M.S. Ghiorso and B.W.E. Structure refinement computations were facilitated by an equipment grant from the Digital Equipment Corporation to M.S. Ghiorso. Support during completion of this manuscript was provided by a National Science Foundation postdoctoral fellowship to M.H. This manuscript benefited from reviews by D. Lattard and L. Ungaretti.

References cited

Bancroft, G.M., Burns, R.G., and Maddock, A.G. (1967) Determination of cation distribution in cummingtonite-grunerite series by Mössbauer spectra. American Mineralogist, 52, 1009–1026.

Barabanov, A.V., and Tomilov, S.B. (1973) Mössbauer study of the isomorphous series anthophyllite-gedrite and cummingtonite-grunerite. Geochemistry International, 10, 1240–1247.

Barrus, R.B. (1970) The petrology of the Precambrian rocks of the High Peaks area, Wind River Mtns., Fremont Co., Wyoming, 86 p. Ph.D. thesis, University of Washington, Seattle, Washington.

Bence, A.E., and Albee, A.L. (1968) Empirical correction factors for microanalysis of silicates and oxides. Journal of Geology, 76, 382–403.

Berg, J.H. (1985) Chemical variations in sodium gedrite from Labrador. American Mineralogist, 70, 1205–1210.

Berman, R.G. (1988) Internally-consistent thermodynamic data for minerals in the system Na_2O-K_2O-CaO-MgO-FeO-Fe_2O_3-Al_2O_3-SiO_2-TiO_2-H_2O-CO_2. Journal of Petrology, 29, 445–522.

Buckley, A.N., and Wilkins, R.W.T. (1971) Mössbauer and infrared study of a volcanic amphibole. American Mineralogist, 56, 90–100.

Burns, R.G., and Strens, R.G.J. (1966) Infrared study of the hydroxyl bands in clinoamphiboles. Science, 153, 890–892.

Cameron, K.L. (1975) An experimental study of actinolite-cummingtonite phase relations, with notes on the synthesis of Fe-rich anthophyllite. American Mineralogist, 60, 375–390.

Cameron, M., and Gibbs, G.V. (1973) The crystal structure and bonding of fluor-tremolite: A comparison with hydroxl tremolite. American Mineralogist, 58, 878–888.

Chernosky, J.V., Jr., and Autio, L.K. (1979) The stability of anthophyllite in the presence of quartz. American Mineralogist, 64, 294–303.

Chernosky, J.V., Day, H.W., and Caruso, L.J. (1985) Equilibria in the system MgO-SiO_2-H_2O. I. Experimental determination of the stability of Mg-anthophyllite. American Mineralogist, 70, 223–236.

Clowe, C.A., Popp, R.K., and Fritz, S.J. (1988) Experimental investigation of the relation between oxygen fugacity, ferric-ferrous ratio and unit cell parameters for four natural clinoamphiboles. American Mineralogist, 73, 487–499.

Domeneghetti, M.C., and Steffen, G. (1992) M1, M2 site populations and

distortion parameters in synthetic Mg-Fe orthopyroxenes from Mössbauer spectra and X-ray diffraction structure refinements. Physics and Chemistry of Minerals, 19, 298–306.

Dyar, M.D. (1984) Precision and interlaboratory reproducibility of measurements of the Mössbauer effect in minerals. American Mineralogist, 69, 1127–1144.

Finger, L.W. (1969) The crystal structure and cation distribution of a grunerite. Mineralogical Society of America Special Paper, 2, 95–100.

Finger, L.W., and Prince, E. (1975) A system of FORTRAN IV computer programs for crystal structure computations. National Bureau of Standards Technology note 854.

Fischer, K.F. (1966) A further refinement of the crystal structure of cummingtonite, $(Mg,Fe)_7(Si_4O_{11})_2(OH)_2$. American Mineralogist, 51, 814–818.

Ghose, S. (1961) The crystal structure of a cummingtonite. Acta Crystallographica, 14, 622–627.

——— (1981) Subsolidus reactions and microstructures in amphibole. In Mineralogical Society of America Reviews in Mineralogy, 9A, 325–372.

——— (1990) Influence of magnetic ordering phenomena on the thermodynamic properties of orthopyroxene and cummingtonite solid solutions. Geological Society of America Abstracts with Programs, 22 (7), A71.

Ghose, S., and Ganguly, J. (1982) Mg-Fe order-disorder in ferromagnesian silicates. In S.K. Saxena, Ed., Advances in physical geochemistry, vol. 2, p. 1–99. Springer-Verlag, New York.

Ghose, S., and Hexiong, Y. (1989) Mn-Mg distribution in a *C2/m* manganoan cummingtonite: Crystal-chemical considerations. American Mineralogist, 74, 1091–1096.

Ghose, S., and Weidner, J.R. (1971a) Oriented transformation of grunerite to clinoferrosilite at 775 °C and 500 bars argon pressure. Contributions to Mineralogy and Petrology, 30, 64–71.

——— (1971b) Mg^{2+}-Fe^{2+} order-disorder in cummingtonite, $(Mg,Fe)_7Si_8O_{22}(OH)_2$ (abs.). Eos, 52, 381.

——— (1972) Mg^{2+}-Fe^{2+} order-disorder in cummingtonite, $(Mg,Fe)_7Si_8O_{22}(OH)_2$: A new geothermometer. Earth and Planetary Science Letters, 16, 346–354.

Greenwood, H.J. (1963) The synthesis and stability of anthophyllite. Journal of Petrology, 4, 317–351.

Hafner, S.S., and Ghose, S. (1971) Iron and magnesium distribution in cummingtonites $(Fe,Mg)_7Si_8O_{22}(OH)_2$. Zeitschrift für Kristallographie, 133, 301–326.

Hawthorne, F.C. (1981) Crystal chemistry of the amphiboles. In Mineralogical Society of America Reviews in Mineralogy, 9A, 1–102.

Hawthorne, F.C., and Grundy, H.D. (1977) The crystal structure and site chemistry of a zincian tirodite by least squares refinement of X-ray and Mössbauer data. Canadian Mineralogist, 15, 309–320.

——— (1978) The crystal chemistry of the amphiboles. VII. The crystal structure and site chemistry of potassian ferri-taramite. Canadian Mineralogist, 16, 53–62.

Hawthorne, F.C., Griep, J.L., and Curtis, L. (1980) A three amphibole assemblage from the Tallan Lake Sill, Peterborough County, Ontario. Canadian Mineralogist, 18, 275–284.

Holland, T.J.B., and Powell, R. (1990) An enlarged and updated internally consistent thermodynamic dataset with uncertainties and correlations: The system K_2O-Na_2O-CaO-MgO-MnO-FeO-Fe_2O_3-Al_2O_3-TiO_2-SiO_2-C-H_2-O_2. Journal of Metamorphic Geology, 8, 89–124.

Ibers, J.A., and Hamilton, W.C., eds. (1974) International tables for X-ray crystallography, vol. 4, p. 99–101 and 149–150. Kynoch, Birmingham, England.

Immega, I., and Klein, C. (1976) Mineralogy and petrology of some metamorphic Precambrian iron formations in southwestern Montana. American Mineralogist, 63, 1116–1144.

Kamineni, D.C. (1973) X-ray and Mössbauer characteristics of a cummingtonite from Yellowknife, district of Mackenzie. Canadian Mineralogist, 12, 230–232.

Kisch, H.J. (1969) Magnesio-cummingtonite, $P2_1/m$: A Ca- and Mn-poor clinoamphibole from New South Wales. Contributions to Mineralogy and Petrology, 21, 319–331.

Klein, C., Jr. (1964) Cummingtonite-grunerite series: A chemical, optical and x-ray study. American Mineralogist, 49, 963–982.

Klein, C., Jr., and Waldbaum, D.R. (1967) X-ray crystallographic properties of the cummingtonite-grunerite series. Journal of Geology, 75, 379–392.

Krupka, K.M., Hemingway, B.S., Robie, R.A., and Kerrick, D.M. (1985) High-temperature heat capacities and derived thermodynamics properties of anthophyllite, diopside, dolomite, enstatite, bronzite, talc, tremolite and wollastonite. American Mineralogist, 70, 261–271.

Lattard, D., and Evans, B.W. (1992) New experiments on the stability of grunerite. European Journal of Mineralogy, 4, 219–238.

Lindemann, W. (1964) Beitrag zur Struktur des Anthophyllits. Fortschritte der Mineralogie, 42, 205.

Maresch, W.V., and Czank, M. (1988) Crystal chemistry, growth kinetics and phase relationships of structurally disordered (Mn^{2+},Mg)-amphiboles. Fortschritte der Mineralogie, 66, 69–121.

Mason, B. (1953) Cummingtonite from the Mikonui River, Westland, New Zealand. American Mineralogist, 38, 862.

Mitchell, J.T., Bloss, F.D., and Gibbs, G.V. (1971) Examination of the actinolite structure and four other *C2/m* amphiboles in terms of double bonding. Zeitschrift für Kristallographie, 133, 273–300.

Mueller, R.F. (1960) Compositional characteristics and equilibrium relations in mineral assemblages of a metamorphosed iron formation. American Journal of Science, 258, 449–497.

Papike, J.J., Ross, M., and Clark, J.R. (1969) Crystal chemical characterization of clinoamphiboles based on five new structure refinements. Mineralogical Society of America Special Paper, 2, 117–136.

Phillips, M.W., Popp, R.K., and Clowe, C.A. (1991) A structural investigation of oxidation effects in air-heated grunerite. American Mineralogist, 76, 1502–1509.

Popp, R.K., Gilbert, M.C., and Craig, J.R. (1977) Stability of Fe-Mg amphiboles with respect to oxygen fugacity. American Mineralogist, 62, 1–12.

Rice, J.M., Evans, B.W., and Trommsdorff, V. (1974) Widespread occurrence of magnesio-cummingtonite, Cima di Gagnone, Ticino, Switzerland. Contributions to Mineralogy and Petrology, 43, 245–251.

Robinson, P., and Jaffe, H.W. (1969) Chemographic exploration of amphibole assemblages from central Massachusetts and southwestern New Hampshire. Mineralogical Society of America Special Paper, 2, 251–274.

Robinson, P., Spear, F.S., Schumacher, J.C., Laird, J., Klein, C., Evans, B.W., and Doolan, B.L. (1982) Phase relations of metamorphic amphiboles: Natural occurrence and theory. In Mineralogical Society of America Reviews in Mineralogy, 9B, 1–227.

Ross, M., Papike, J.J., and Shaw, J.J. (1969) Exsolution textures in amphiboles as indicators of subsolidus thermal histories. Mineralogical Society of America Special Paper, 2, 275–299.

Seifert, F. (1978) Equilibrium Mg-Fe^{2+} cation distribution in anthophyllite. American Journal of Science, 278, 1323–1333.

Seifert, F., and Virgo, D. (1974) Temperature dependence of intra-crystalline Fe^{2+}-Mg distribution in a natural anthophyllite. Carnegie Institution of Washington Year Book, 73, 405–411.

Shannon, R.D., and Prewitt, C.T. (1969) Effective ionic radii for oxides and halides. Acta Crystallographica, B25, 925–946.

Skogby, H., Annersten, H., Domeneghetti, M.C., Molin, C.M., and Tazzola, V. (1992) Iron distribution in orthopyroxene: A comparison of Mössbauer spectroscopy and X-ray refinement results. European Journal of Mineralogy, 4, 441–452.

Smelik, E.A., and Veblen, D.R. (1993) A transmission and analytical electron microscope study of exsolution microstructure and mechanisms in the orthoamphiboles anthophyllite and gedrite. American Mineralogist, 78, 511–532.

Sueno, S., Papike, J.J., Prewitt, C.T., and Brown, G.E. (1972) Crystal chemistry of high cummingtonite. Journal of Geophysical Research, 77, 5767–5777.

Ungaretti, L., Smith, D.C., and Rossi, G. (1981) Crystal chemistry by X-ray structure refinement and electron microprobe analysis of a series of sodic-calcic to alkali amphiboles from the Nybo eclogite pod, Norway. Bulletin de Mineralogie, 104, 400–412.

Veblen, D.R., and Burnham, C.W. (1978) New biopyriboles from Chester, Vermont. I. Descriptive mineralogy. American Mineralogist, 63, 1000–1009.

Viswanathan, K., and Ghose, S. (1965) The effect of Mg^{2+}-Fe^{2+} substi-

tution on the cell dimensions of cummingtonites. American Mineralogist, 50, 1106–1112.

Walitzi, E.M., Walter, F., and Ettinger, K. (1989) Verfeinerung der Kristallstruktur von Anthophyllit vom Ochsenkogel/Gleinalpe, Oesterreich. Zeitshrift für Kristallographie, 188, 237–244.

Walter, L.S., and Salisbury, J.W. (1989) Spectral characterization of igneous rocks in the 8- to 12 μm region. Journal of Geophysical Research, 94 (B7), 9203–9213.

Yakovleva, A.K., Yegorova, L.N., and Litvin, A.L. (1978) Magnesiocummingtonite with primitive cell $P2_1/m$. International Geology Review, 20, 1357–1362.

Ying, Y., Li, Y., and Sun, C. (1989) Fe^{2+} site occupancy in cummingtonite-grunerite and estimation of equilibrium temperature. Chinese Science Bulletin, 34 (23), 1975–1979.

Zhang, L., Ahsbachs, H., Kutoglu, A., and Hafner, S.S. (1992) Compressibility of grunerite. American Mineralogist, 77, 480–483.

Manuscript received October 13, 1993
Manuscript accepted April 25, 1994